Influence of the Extratropical Ocean Circulation on the Intertropical Convergence Zone in an Idealized Coupled General Circulation Model

NEVEN S. FUČKAR

International Pacific Research Center, University of Hawaii at Manoa, Honolulu, Hawaii

SHANG-PING XIE

International Pacific Research Center, and Department of Meteorology, University of Hawaii at Manoa, Honolulu, Hawaii, and Scripps Institution of Oceanography, University of California, San Diego, La Jolla, California

RICCARDO FARNETI

Earth System Physics Section, International Centre for Theoretical Physics, Trieste, Italy

ELIZABETH A. MAROON AND DARGAN M. W. FRIERSON

Department of Atmospheric Sciences, University of Washington, Seattle, Washington

(Manuscript received 25 May 2012, in final form 19 December 2012)

ABSTRACT

The authors present coupled model simulations in which the ocean's meridional overturning circulation (MOC) sets the zonal mean location of the intertropical convergence zone (ITCZ) in the hemisphere with deep-water production. They use a coarse-resolution single-basin sector coupled general circulation model (CGCM) with simplified atmospheric physics and two idealized land–sea distributions.

In an equatorially symmetric closed-basin setting, unforced climate asymmetry develops because of the advective circulation–salinity feedback that amplifies the asymmetry of the deep-MOC cell and the upper-ocean meridional salinity transport. It confines the deep-water production and the dominant extratropical ocean heat release to a randomly selected hemisphere. The resultant ocean heat transport (OHT) toward the hemisphere with the deep-water source is partially compensated by the atmospheric heat transport (AHT) across the equator via an asymmetric Hadley circulation, setting the ITCZ in the hemisphere warmed by the ocean.

When a circumpolar channel is open at subpolar latitudes, the circumpolar current disrupts the poleward transport of the upper-ocean saline water and suppresses deep-water formation poleward of the channel. The MOC adjusts by lowering the main pycnocline and shifting the deep-water production into the opposite hemisphere from the channel, and the ITCZ location follows the deep-water source again because of the Hadley circulation adjustment to cross-equatorial OHT. The climate response is sensitive to the sill depth of the channel but becomes saturated when the sill is deeper than the main pycnocline depth in subtropics. In simulations with a circumpolar channel, the ITCZ is in the Northern Hemisphere (NH) because of the Southern Hemisphere (SH) circumpolar flow that forces northward OHT.

1. Introduction

A developing line of research investigates the influence of various extratropical perturbations on the mean global climate through the interhemispheric thermal gradient and specifically on the tropical circulation and precipitation. Early motivation includes the goal to understand the nature of abrupt climate changes during glacial periods in the late Quaternary (Dansgaard et al. 1993). The rapid warming and cooling over the North Atlantic, recorded in Greenland ice cores (Grootes and Stuiver 1997), are reflected in the tropical Atlantic (Peterson et al. 2000; Wang et al. 2004) and the east Pacific (Koutavas and

Corresponding author address: Neven S. Fučkar, IPRC/SOEST, University of Hawaii at Manoa, 1680 East-West Rd., POST Bldg. 401, Honolulu, HI 96822.
E-mail: nevensf@gmail.com.

DOI: 10.1175/JCLI-D-12-00294.1

Lynch-Stieglitz 2004). Millennial-scale variations in these tropical paleoclimate records can be interpreted as the result of southward (northward) rainfall shifts during rapid cooling (warming) in the north: this is typically hypothesized to stem from weakening (strengthening) of the Atlantic meridional overturning circulation (MOC; e.g., Broecker et al. 1985).

Proxy records and observations will always contain gaps; hence their combination with models provides a more complete understanding. Changes in high-latitude land and sea ice cover in AGCM–slab ocean models generate an interhemispheric thermal difference that shifts the global tropical precipitation away from the cooled hemisphere (Chiang and Bitz 2005; Broccoli et al. 2006). In a series of coupled general circulation model (CGCM) experiments, an Atlantic MOC disruption, due to additional freshwater input in the northern Atlantic, manifests various degrees of Northern Hemisphere (NH) cooling and southward displacement of the intertropical convergence zone (ITCZ; Manabe and Stouffer 1995; Zhang and Delworth 2005; Timmermann et al. 2007, Drijfhout 2010). Modeling studies of industrial aerosol emissions, primarily originating in the NH, show that these tend to increase the reflectivity of the atmosphere (because of higher scattering and cloud albedo) and induce NH-wide cooling that shifts the ITCZ south and weakens the NH summer monsoons (Yoshimori and Broccoli 2008).

Realistic model geometries sometimes mask the key processes and pathways from being distinctly revealed. An idealized geometry under hypothetical conditions can build our knowledge at a more fundamental level. For example, in a set of AGCM–slab ocean models without land, prescribed extratropical mixed layer heating representing the ocean heat transport (OHT) affects the tropical mean state and confirms the sensitivity of the ITCZ position to the interhemispheric thermal gradient (Kang et al. 2008, 2009): the zonal average maximum precipitation in the tropics moves away from (toward) the cooled (warmed) hemisphere.

Studies about the remote influence of the extratropics on the global interhemispheric climate asymmetry enrich our understanding of the dynamics of the Hadley circulation and the ITCZ (e.g., Held and Hou 1980; Xie and Philander 1994; Philander et al. 1996). The specific configurations of the eastern coastline, stratus clouds, and the air–sea feedbacks are the key local controlling factors in the tropics (Xie 2004). We aim to contribute to a more encompassing dynamical picture of tropical climate as the superposition of local and remote processes. Our focus is on elements of the ocean dynamics that connect upper-ocean horizontal circulation with the MOC, which can induce a change in the extratropical surface heating that can modify tropical climate. The Southern Ocean circumpolar flow is the key dynamical interhemispheric difference throughout the world oceans with crucial effects on the earth's climate. Various geometries of the Drake Passage[1] in OGCM and OGCM–atmosphere energy balance setups (e.g., Cox 1989; Toggweiler and Bjornsson 2000; Sijp and England 2004) lead to a substantially different MOC, OHT, and interhemispheric thermal gradient. Our paper goes forward by employing both a dynamically resolved ocean and atmosphere in an idealized geometry similar, in approach, to Smith et al. (2006) and Ferreira et al. (2010).

We examine the influence of internally excited or externally forced change in extratropical ocean circulation on the mean climate and particularly on aspects of the tropical circulation and precipitation in an idealized coupled numerical setup. Section 2 describes our simplified CGCM, outlines a series of experiments, and presents the control case. Section 3 focuses on unforced interhemispheric symmetry breaking in a closed-basin symmetric configuration. Section 4 studies forced symmetry breaking via opening a circumpolar channel with different sill depths in different hemispheres. Sections 5 and 6 summarize our main results that further understanding of remote processes controlling elements of the tropical climate and discuss possible future directions.

2. Numerical setup and the control experiments

Developing insight into such a complex system as the planetary climate requires analysis and modeling of various domains at different levels of complexity (Held 2005). We employ a fully dynamical intermediate complexity climate model (ICCM) unburdened by realistic land distribution and complex atmospheric physics. Our ICCM setup is derived from the Geophysical Fluid Dynamics Laboratory Climate Model version 2.0 (GFDL CM2.0; Delworth et al. 2006) in a modular way through a set of parameterization and geographic simplifications (Farneti and Vallis 2009; Vallis and Farneti 2009). ICCM is publically available from GFDL as a part of CM2 distribution (https://fms.gfdl.noaa.gov/gf/).

a. Elements of idealized climate system

This CGCM solves the three-dimensional primitive equations for the atmosphere and ocean with a dynamically consistent surface exchange of momentum, heat, and freshwater fluxes, but it uses simplified atmospheric physics. We select an idealized coarse-resolution

[1] The narrow body of water between Patagonia and the Antarctic Peninsula.

configuration with a sector atmosphere over land without mountains and a single-basin flat-bottom ocean. The goal is to expose crucial elements of coupled dynamics in a more revealing geometrical setting and to make the model computationally less demanding.

The atmospheric component, with 7 vertical levels and 3.75° × 3° horizontal resolution, has a sector geometry that is 120° long and spans from 84°S to 84°N. This AGCM is based on a moist B-grid dynamical core, but it uses a gray radiation scheme with the longwave flux independent of water vapor and clouds (Frierson et al. 2006). The model is forced with a time-independent, zonally uniform, top-of-atmosphere solar radiation that analytically mimics the observed mean profile. Solar absorption in the atmosphere is neglected and longwave optical depth has prescribed annual mean distribution. A large-scale condensation scheme is applied along with a simplified Betts–Miller convection scheme (Betts 1986; Frierson 2007); thus, humidity and temperature are adjusted when saturation occurs and precipitation falls out immediately (there is no liquid water or clouds in the atmosphere). Eliminating water vapor and cloud feedbacks (radiative fluxes depend only on temperature) enables us to focus on a purely dynamical response of the coupled climate system to the ocean state change.

The ocean component is the Modular Ocean Model (MOM) version 4.0 (Griffies et al. 2004) with 24 vertical levels (of thickness ranging from 10 m at the top to 315 m at the bottom) and 2° × 2° horizontal resolution. The ocean basin is 60° wide, spans from 70°S to 70°N, and has a flat bottom that is 3.9 km deep. Circumpolar channels with various sill depths are opened in the subpolar regions of both hemispheres to explore the impact of high-latitude zonally unconstrained flows. The ocean physics parameterizations are similar to the standard free surface MOM model incorporated in CM2.0. This OGCM has constant vertical tracer diffusivity of 0.5 $cm^2\ s^{-1}$. It applies the Gent–McWilliams (GM) skew flux scheme combined with a downgradient neutral diffusion that parameterizes the effects of mesoscale eddies using constant eddy tracer diffusivity of 800 $m^2\ s^{-1}$ (Gent and McWilliams 1990; Griffies 1998).

The dynamic–thermodynamic sea ice simulator (SIS; Winton 2000) is coupled within the ocean grid. The land model LM2.0 is configured with the atmospheric horizontal resolution. It is implemented as a collection of soil water reservoirs with constant water availability and heat capacity at each land cell. The excess precipitated water is redistributed back to the ocean at a nearby grid point. There are no mountains or glaciers, and surface albedo values are altered to obtain a realistic mean climate in the control experiments [for more details of ICCM setup, see Farneti and Vallis (2009)].

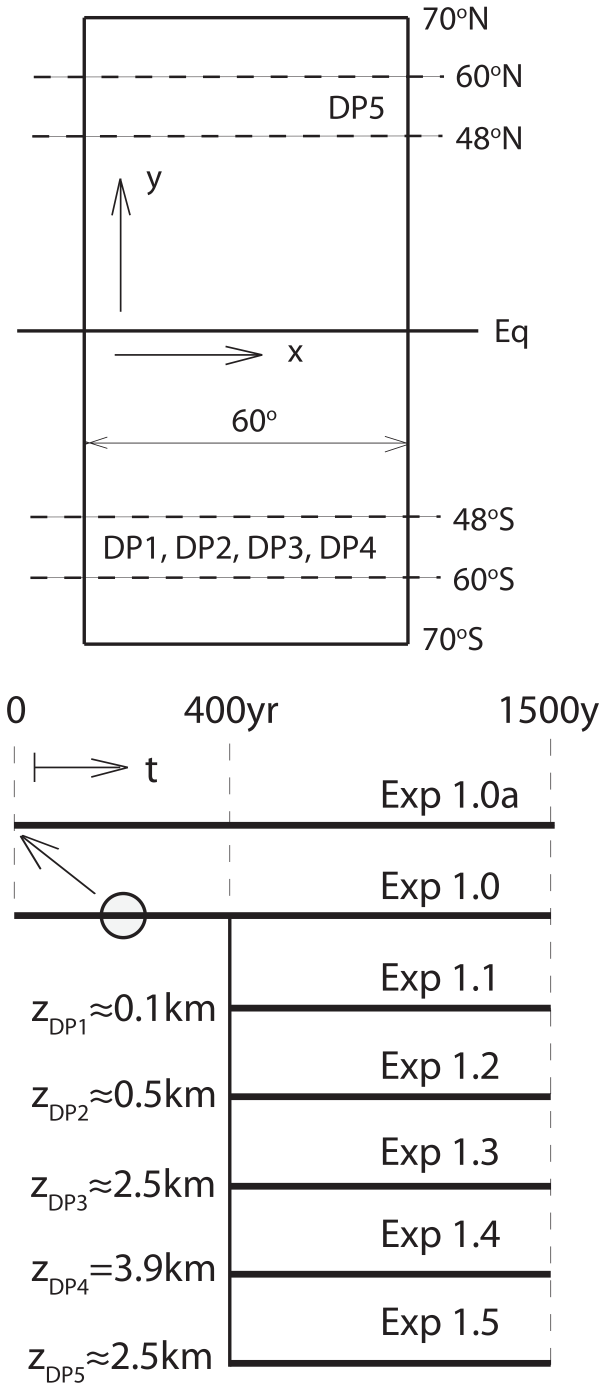

FIG. 1. (top) The different ocean basin geometries used in this study and (bottom) time integration outline for the whole series of experiments (lower panel).

b. The role of ocean basin geometry

The only external forcing agent of the interhemispheric asymmetries in our experiments is the ocean basin geometry through different configurations of a circumpolar channel. Figure 1 shows a schematic map and key geometric

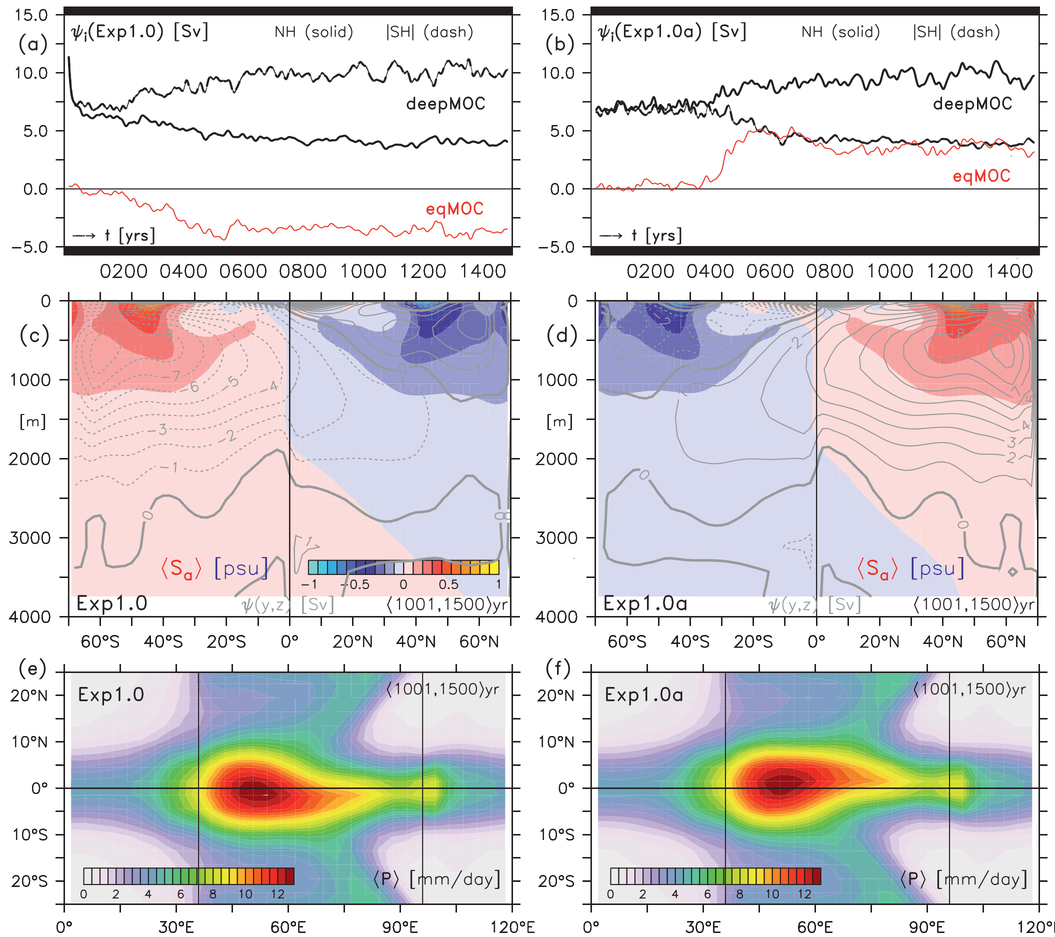

FIG. 2. (top) Time evolution (smoothed with the 31-yr Hamming filter) of MOC streamfunction indices in (a) Exp1.0 and (b) Exp1.0a. Here, "deepMOC" (black curves) is the magnitude of the deep-MOC cell (subsurface extremum in the extratropics) and "eqMOC" (red curves) is the amplitude of deep-water exchange across the equator (subsurface extremum). The absolute values of the SH MOC indices (dashed curves) are shown for easier comparison of the interhemispheric differences. (middle) The MOC streamfunction (gray contours), with positive values representing clockwise circulation, over the zonally averaged anomalous salinity (shading), with respect to the symmetrized mean control state, averaged over the last 500 yr of (c) Exp1.0 and (d) Exp1.0a. (bottom) Tropical precipitation averaged over the last 500 yr of (e) Exp1.0 and (f) Exp1.0a.

parameters of various ocean basins, as well as 1500-yr integration timeline of our suite of experiments. The two control experiments, Exp1.0 and Exp1.0a, have an equatorially symmetric configuration with a closed ocean basin. They are initialized from no-flow symmetric initial conditions (IC) of potential temperature and salinity. Exp1.0 has zonally uniform IC with a prescribed main pycnocline. Exp1.0a starts from dynamically quasi-balanced IC obtained from Exp1.0 outputs by using only the symmetric components (averaged from year 151 to 200). After 400 yr of Exp1.0 integration, we branch an additional set of tectonically forced experiments through the sudden opening of circumpolar channels (between 48° and 60° latitude) with various sill depths. Specifically, Exp1.1, Exp1.2, Exp1.3, and Exp1.4 have an idealized Drake Passage 102, 480, 2436, and 3900 m deep, respectively, while Exp1.5 features the NH equivalent that is 2436 m deep.

The unbalanced symmetric IC of Exp1.0 yields, from the start, a fast dynamical adjustment and strong fluctuations that lead to a deep-MOC asymmetry after about 50 yr (Fig. 2a). Specifically, in Exp1.0 the deep water is predominately produced in the Southern Hemisphere (SH; dashed black curve) and exported to the NH (red curve). The symmetric geometry and forcing of the control cases require the ensemble mean control climate to be symmetric. Different experiments started from different IC should manifest climate asymmetry with various, randomly selected, interhemispheric signs. Exp1.0a (Fig. 2b) develops the opposite sign of deep-MOC asymmetry at

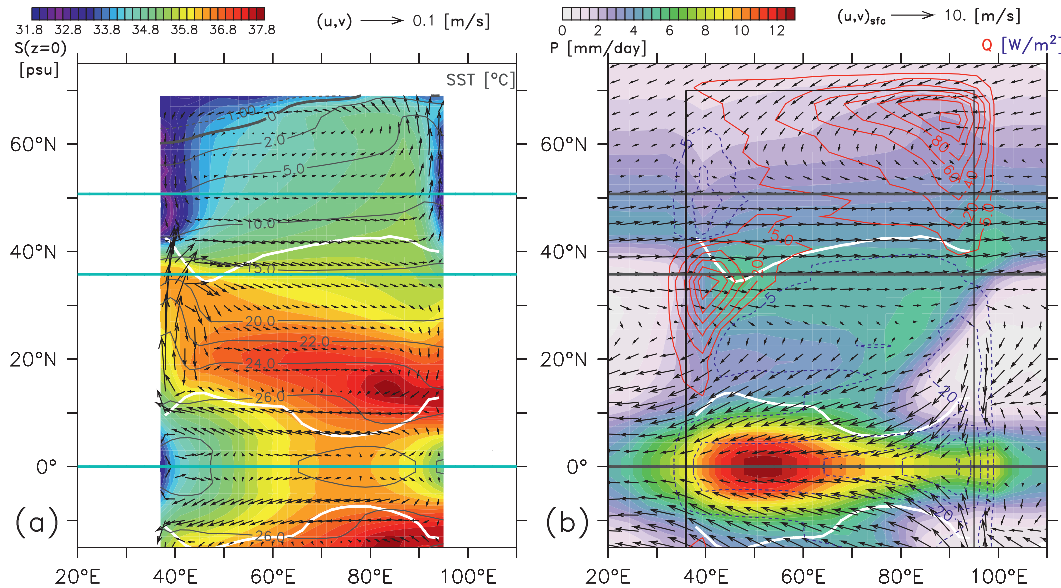

FIG. 3. The symmetrized mean control climate averaged over the last 100 yr of Exp1.0 and Exp1.0a. (a) Surface salinity (shading), surface currents averaged over top 100 m (vectors), and SST (gray contours). (b) Precipitation (shading), surface level winds (vectors), and net surface heat flux [red (positive into the atmosphere) and blue (negative out of the atmosphere) contours]. The SH conditions mirror the presented NH conditions across the equator by construction. White contours mark boundaries between ocean gyres (zero wind stress curl), while green (gray) horizontal lines in (a) [(b)] delineate surface boundaries between the meridional overturning cells in the atmosphere (the zonally averaged position of zero surface meridional wind).

a rate slower than Exp1.0. The two control experiments reach equatorially mirrored asymmetric final steady states of the ocean (see the middle panels in Fig. 2): they demonstrate the ocean bistability of our symmetric coupled system that is reflected in, among other things, tropical precipitation asymmetry. The bottom panels in Fig. 2 show that the maximum of tropical precipitation is in the hemisphere with the main deep-water source.

c. *The symmetrized mean control state*

In general, any continuous and finite variable can be decomposed into the sum of equatorially symmetric and antisymmetric parts.[2] We use the set of long-term averages of symmetric or antisymmetric field components from Exp1.0 and Exp1.0a to approximate the ensemble mean control climate of a large number of closed-basin symmetric experiments. We present below some fields of this symmetrized mean control state (averaged over the last 100 yr of integration) that are important for the analysis of asymmetries in the rest of the paper.

The surface ocean circulation (averaged over the top 100 m) in Fig. 3a shows tropical, subtropical, and subpolar gyres divided by zero wind stress (white) contours. The subpolar gyres are too wide in comparison to the real-world North Atlantic because of an equatorward bias of the midlatitude westerlies (Fig. 3b). The SST (contours in Fig. 3a) and surface salinity (shading in Fig. 3a) distributions show the influence of precipitation patterns (shading in Fig. 3b), surface currents (vectors in Fig. 3a), and surface winds (vectors Fig. 3b). The green (gray) horizontal lines in Fig. 3a (Fig. 3b) mark the surface borders between the Hadley, Ferrel, and polar cells. The red (positive) and blue (negative) contours in Fig. 3b show the net surface heat flux distribution (positive upward). This distribution clearly reflects the influence of strong boundary currents in the extratropical regions that coincide with a strong SST gradient and primarily yield a strong heat release from the ocean.

The mean control climate in Fig. 4a shows a meridional overturning mass streamfunction clearly displaying the atmospheric overturning cells. Figure 4b delineates the meridional distribution of the total planetary (black curve) and ocean (blue curve) energy transport along with the atmospheric moist static (red curve), dry static (purple curve), and latent (green curve) energy transports. The decomposition of energy transport confirms

[2] For example, $SST(y) = [SST(y) + SST(-y)]/2 + [SST(y) - SST(-y)]/2 = SST_s(y) + SST_a(y)$, where $SST_s(-y) = SST_s(y)$ and $SST_a(-y) = -SST_a(y)$. The basic equatorially symmetrized component of some fields is symmetric (θ, S, q, u, etc.), while in others it is antisymmetric (v, ψ, etc.).

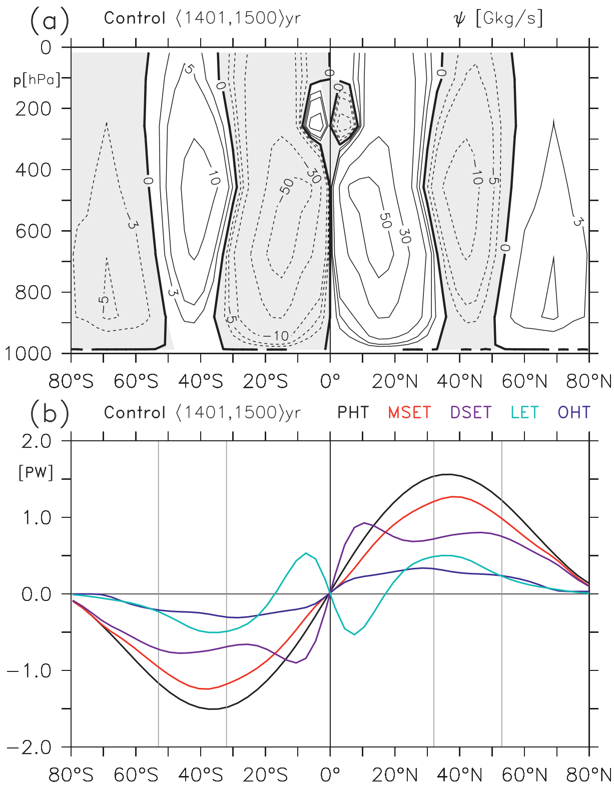

FIG. 4. The symmetrized mean control climate averaged over the last 100 yr of Exp1.0 and Exp1.0a. (a) Atmospheric meridional overturning streamfunction (contours and gray shading for negative values). (b) Meridional heat transport elements: total planetary (black curve), moist static energy (red curve), dry static energy (purple curve), latent energy (green curve), and ocean (blue curve). Vertical gray lines in (b) mark surface boundaries of the Hadley, Ferrel, and polar overturning cells (the zonally averaged position of zero surface meridional wind).

that the latent heat transport (primarily in the lower troposphere because of high specific humidity) is opposing the dominant dry static energy transport in the deep tropics, which is in the direction of the upper branch of the thermally direct Hadley cell (Held 2001; Trenberth and Stepaniak 2003). The realized values of the meridional heat transport components are approximately one-third of the real-world values, which is expected since the sector atmosphere is only 120° wide.

3. Unforced symmetry breaking

The possibility of multiple ocean equilibria, arising because of nonlinear interactions between ocean circulation and salinity and because of the inherent differences in heat and freshwater ocean–atmosphere coupling, has been studied for some time (e.g., Bryan 1986; Marotzke and Willebrand 1991; Dijkstra and Molemaker 1997; Dijkstra and Ghil 2005; Den Toom et al. 2012). The symmetry breaking and dominance of deep-water production in one hemisphere is caused by the advective ocean circulation–salinity feedback (Stommel 1961; Rooth 1982). An increase of surface salinity in the subpolar region of one hemisphere relative to the other causes a local intensification of deep-water production: this leads to export of an excess of deep water to the other hemisphere and asymmetry in the deep-MOC cell. Its surface branch advects additional subtropical high-salinity water toward the subpolar region with intensified deep-water production and further increases local surface salinity, acting as a positive feedback.

Internal variability spontaneously initiates the MOC asymmetry in our control closed-basin numerical setup. For example, Fig. 2b shows that Exp1.0a gradually develops the dominant source of deep-water production in the NH (solid black curve) and deep southward return flow across the equator (red curve). In the next subsection, we analyze the time evolution of zonally collapsed surface anomalies, with respect to the symmetrized mean control state, critical for the development of an interhemispheric asymmetry in the MOC.

a. *Development of key surface anomalies in a control experiment*

Shading in Fig. 5a shows the key phase (from Fig. 2b) of the development of the anomalous northward upper-ocean salinity transport. Its directional synchronization across the equator triggers and amplifies the deep-MOC asymmetry. It strives to amplify the asymmetry in surface salinity and thus in surface density that positively feedbacks on the deep-MOC asymmetry, most importantly in the extratropics. This nonlinear characteristic is the crucial reason for the existence of multiple equilibria in our symmetric configuration. A decrease (increase) of surface salinity in the SH (NH) extratropics in Fig. 5b coincides with a decrease (increase) of SST in Fig. 5c also caused by anomalous northward upper-ocean transport. The growth of subpolar SST anomalies limits the surface density anomalies and magnitude of the deep-MOC asymmetry. On oceanic long time scales in the extratropics SST anomalies induce anomalies in net surface heat flux (shading in Fig. 5d) that strive to damp SST anomalies (they have the same sign in Figs. 5c,d). The surface heat flux anomalies, in contrast to SST anomalies, have predominately opposite signs across 36° latitude (poleward boundary of the Hadley cell) in each hemisphere and much greater amplitudes in the extratropics than in the tropics, indicating that the extratropics are the source of an interhemispheric thermal gradient.

The moderate anomalies in SST (Fig. 5c) and net surface heat flux (Fig. 5d) located close to the poleward

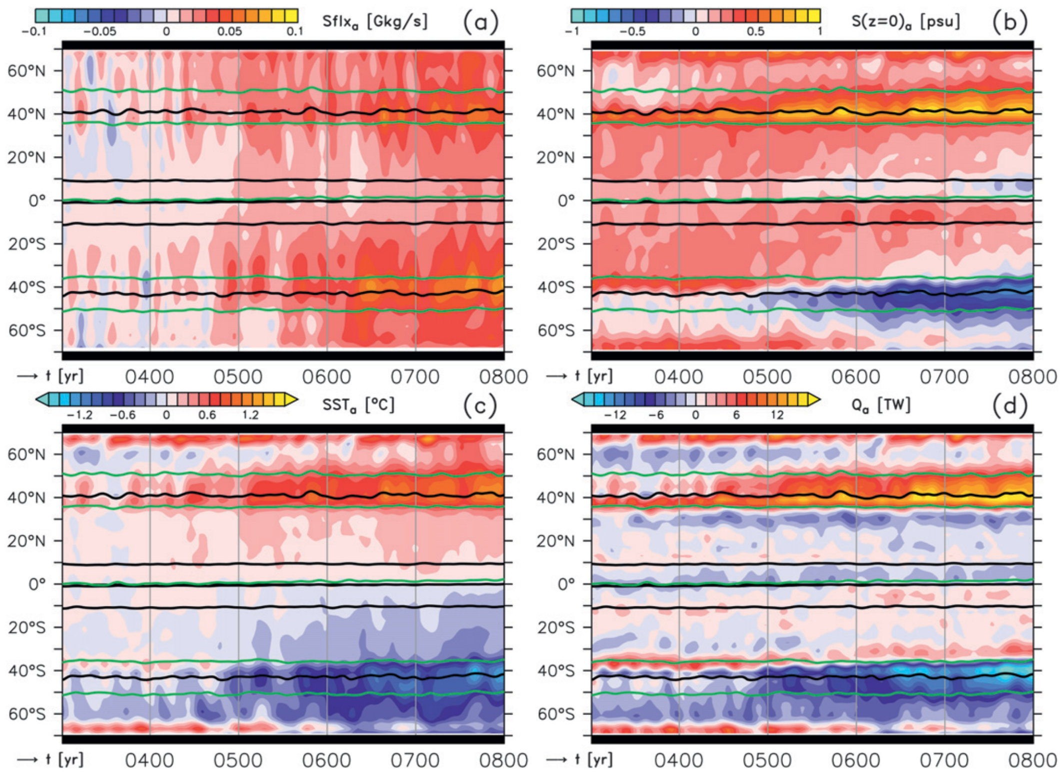

FIG. 5. A key segment of the evolution of anomalous components, with respect to the symmetrized mean control fields, in Exp1.0a: (a) anomaly of meridional salinity mass flux zonally and vertically integrated in top 200 m (10^9 kg s^{-1}), (b) zonally averaged anomaly of surface salinity (psu), (c) zonally averaged anomaly of SST (°C), and (d) zonally and 3° meridionally integrated anomaly of net surface heat flux (10^{12} W). The green curves mark zonal mean surface boundaries between the Hadley, Ferrel, and polar cells, while the black curves mark zonal mean boundaries between the tropical, subtropical, and subpolar gyres. The 31-yr Hamming filter is applied to all fields. The surface heat flux from the ocean to the atmosphere has positive sign.

edges of the ocean basin beneath the polar cell directly reflect the asymmetry in deep-water production. However, the locations of the strongest anomalies in all surface scalar fields in Fig. 5 are in the vicinity of subtropical-subpolar divide (which is marked by the black contours fluctuating about 42° latitude) beneath the Ferrel cell (which is located between midlatitude green contours). Hence, the anomalous meridional upper-ocean salinity transport, a key element of the advective feedback, plays the most important role first during the poleward transition of upper-ocean water from the subtropical to the subpolar gyre and then when reaching high-latitude site of deep-water formation.

b. *Final steady-state surface conditions of a control experiment*

The distribution of surface salinity asymmetry in the final steady state of Exp1.0a in Fig. 6a shows two key boundary regions with the most pronounced anomalies in the extratropics: the extended region of convergence of the subtropical and subpolar western boundary currents and the eastern poleward sector of the subpolar domain. The anomalies in these particular regions arise because of surface current anomalies (vectors in Fig. 6a) acting across the strong gradient in the mean surface salinity (shading in Fig. 3a). Northward current anomalies along the entire western boundary and subpolar eastern boundary constitute the key contributions to the northward surface branch of the deep pole-to-pole MOC cell in Fig. 2d.

Where the surface salinity has a large asymmetry in the extratropics, there is also a large asymmetry in SST (contours in Fig. 6a). It arises where strong anomalous surface currents also cross the regions with a strong SST gradient in the control state (contours in Fig. 3a). Extratropical SST anomalies strongly force the atmosphere primarily through anomalies in latent heat flux (contours in Fig. 6b). In Exp1.0a anomalously high NH (low SH) SST in the extratropics leads to anomalous release (uptake) of heat from (by) the ocean. Sensible heat flux asymmetry has the same sign as the latent heat flux asymmetry under the Ferrel cell but much weaker

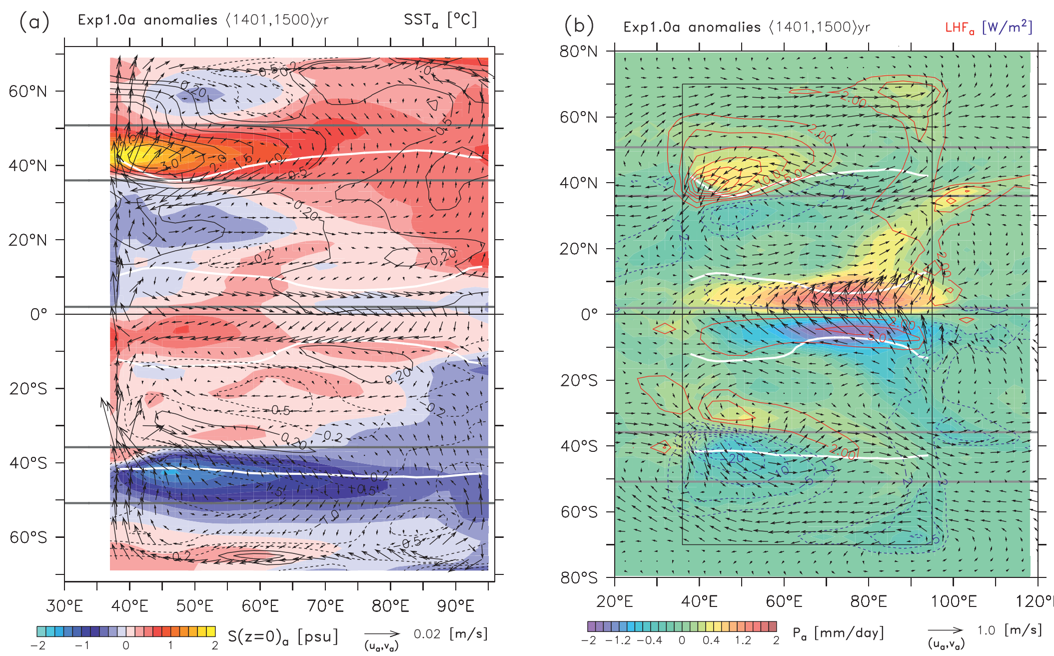

FIG. 6. The steady-state anomalies, with respect to the symmetrized mean control state in Fig. 3, averaged over the last century of Exp1.0a. (a) Anomalous SST (contours), anomalous surface salinity (shading), and anomalous surface currents averaged over the top 100 m (vectors). (b) Anomalous latent heat flux [red (positive in the atmosphere) and blue (negative out of the atmosphere), contours], anomalous precipitation (shading), and anomalous surface wind (vectors). The gray horizontal lines mark zonal mean surface boundaries between the Hadley, Ferrel, and polar cells (zonal average of zero meridional surface wind), while the white curves mark boundaries between the tropical, subtropical, and subpolar gyres (zero wind stress curl).

amplitude (not shown). The deep pole-to-pole MOC imposes the interhemispheric thermal gradient in the atmosphere most significantly at these two specified extratropical regions. Surface air temperature (SAT) asymmetry (not shown) closely mimics patterns of SST asymmetry. In the tropics, a weaker surface heat flux asymmetry with the opposite sign in the tropics is forced from the extratropics through local surface wind change as described in the next subsection.

c. *Dynamic response of the atmosphere to the ocean asymmetry*

The asymmetric surface heating of the extratropical atmosphere influences the tropics by generating a local interhemispheric thermal gradient via large-scale eddy heat fluxes (Kang et al. 2008, 2009) and surface wind–evaporation–SST (WES) coupling in the region of the low-latitude easterlies (Chiang and Bitz 2005; Chiang et al. 2008). The low-latitude coupled atmosphere–ocean system responds by inducing an anomalous cross-equatorial Hadley cell (Fig. 7b). This cell facilitates the cross-equatorial atmospheric heat transport (AHT) from the warmer to the colder hemisphere (red curve in Fig. 7c) ultimately as a response to the cross-equatorial OHT from the colder to warmer hemisphere (blue curve in Fig. 7c). Since the Hadley circulation is thermally direct (e.g., Dima and Wallace 2003; Webster 2004), the surface branch of the anomalous cell extends across the equator (Fig. 7b), providing anomalous low-level moisture transport toward the warmer hemisphere (green curve in Fig. 7c). Tropical coupled atmosphere–ocean dynamics push the ascending branch of the anomalous Hadley cell and the maximum of tropical precipitation (shadings in Figs. 2f, 6b and blue curve in Fig. 7a) to the warmer hemisphere with the main source of deep-water production. In the extratropics, asymmetry in precipitation (shading in Fig. 6b), induced by the asymmetry in latent heat flux (contours in Fig. 6b), is opposing the asymmetry in surface salinity (shading in Fig. 6a). However, the anomalous surface circulation (vectors in Fig. 6a) across a strong gradient in the mean surface salinity is more important for maintaining the surface salinity anomaly. There is more tropical precipitation in the hemisphere with increased extratropical salinity and hence tropical rainfall asymmetry is also ineffectively opposing the upper-ocean anomalous salinity transport and the deep-MOC asymmetry.

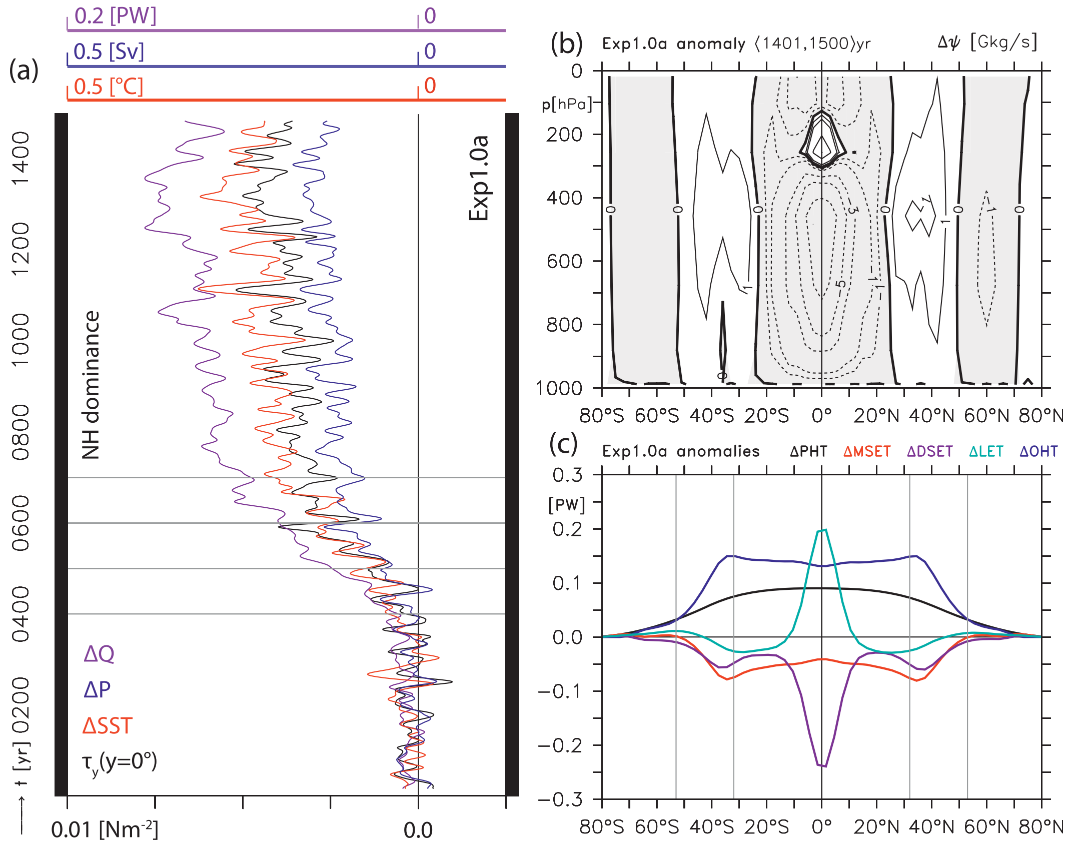

FIG. 7. (a) Time evolution (with applied 31-yr Hamming filtering) of the following asymmetry parameters in Exp1.0a: the black curve is zonal mean meridional wind stress at the equator (N m^{-2}), the red curve is difference between (0°, 10°N)–averaged SST and (10°S, 0°)–averaged SST (in °C), the blue curve is difference between (0°, 10°N)–integrated precipitation and (10°S, 0°)–integrated precipitation (Sv; 1 Sv ≡ 10^6 m^3 s^{-1}), and the purple curve is integrated asymmetry of extratropical surface heat flux with positive values representing excess heat release into the NH atmosphere (PW). (b),(c) Anomalous (with respect to symmetrized control state in Fig. 4) overturning streamfunction in the atmosphere and meridional heat transport components averaged over the last 100 yr. In (c) blue, black, red, purple, and green curves show vertically and zonally integrated anomalous ocean heat, total planetary heat, moist static energy, dry static energy, and latent energy transport, respectively.

Figure 7a shows that the buildup of the extratropical surface heat flux asymmetry[3] (purple curve with NH maximum) very gradually excites coherent tropical asymmetries with the same sign. This is characteristic of the deep-MOC-guided mechanism of the tropical–extratropical and interhemispheric interaction. In the tropics, the WES feedback (Xie 2004) plays an important role in the local coupling of cross-equatorial wind stress (solid black curve showing average northward direction in Fig. 7a), SST asymmetry (red curve with NH maximum in Fig. 7a), and cumulative precipitation asymmetry[4] (blue curve with NH maximum in Fig. 7a). The cross-equatorial ‘‘C shape’’ of anomalous surface wind in Fig. 6b is a signature of the WES feedback that in Exp1.0a connects the SH zone of stronger easterlies, stronger evaporation, and lower SST with the NH zone of weaker easterlies, weaker evaporation, and higher SST on short time scales.

The sign and magnitude of tropical anomalies on multidecadal and longer time scales in our model is controlled by the extratropical latent heat flux anomalies. In Exp1.0a,

[3] The asymmetry index of total extratropical net surface heat flux is defined as the half of the difference between total surface heat flux in the extratropics of the NH and the SH. Surface heat flux is positive upward, so positive (negative) values of this asymmetry index represent excess ocean heat release in the NH (SH) extratropics.

[4] We define it as the total precipitation in the NH deep tropics, between the equator and 10°N, minus the total precipitation in the SH deep tropics, between 10°S and the equator, Positive (negative) values occur if the ITCZ is in the NH (SH).

a boosted (suppressed) extratropical heat release in the NH (SH) atmosphere makes it, in a thermal sense, the summer-like (winter-like) hemisphere with a weaker (stronger) jet stream due to a decrease (increase) in the meridional surface temperature gradient between the equator and extratropics. The Hadley, Ferrel, and polar cells in the NH (SH) get weaker (stronger) in Fig. 7b and manifest the associated asymmetries in the surface winds: weakening (strengthening) in the NH (SH) in Fig. 6b. In the tropics, southerly cross-equatorial surface wind and weaker (stronger) easterlies in the NH (SH) yield a weaker (stronger) latent heat flux that leads to a negative (positive) tropical surface heat flux anomaly in Fig. 5d. This in turn produces higher (lower) tropical SST in Fig. 5c. On the other hand, weaker (stronger) midlatitude westerlies in the NH (SH) in Exp1.0a reduce (enhance) equatorward Ekman transport between the subpolar and subtropical gyre and thus amplify the anomalous northward upper-ocean transport: that is, the surface branch of the pole-to-pole deep-MOC cell.

Similar unforced symmetry breaking on oceanic long time scales is realized in the evolution of Exp1.0 but in the opposite direction (Fig. 2). Our symmetric setup clearly manifests climate bistability. We bring our study a step closer to the real-world geometry by opening various circumpolar channels in the next section.

4. Forced symmetry breaking

We mechanically force changes in our coupled system through modifications of the basin boundaries in time. Specifically, the sudden opening of various circumpolar channels in Exp1.1 through Exp1.5 (starting from Exp1.0 after 400 yr of integration) forces an asymmetry in the extratropical upper-ocean circulation and the MOC. In this section, we examine the impact of the circumpolar current on the MOC and tropical climate and whether the coupled system responds in a similar way as in the closed-basin experiments.

a. *Development of key surface anomalies in a forced experiment*

Exp1.3 opens an approximately 2.5-km-deep SH circumpolar channel (the closest to the Drake Passage in our set of open-basin experiments). The initial development of anomalous southward upper-ocean salinity transport from Exp1.0 very quickly reverses in the SH after the channel opens (shading in Fig. 8a). The rapidly formed circumpolar flow prevents establishment of a net zonal pressure gradient; hence, it constrains the geostrophic component of the circulation to have zero net meridional flow above the sill level and suppresses meridional transport. The parameterized GM mesoscale eddy transport is only weakly changed with the change in stratification, but it is of secondary importance in our model. Substantial weakening of southward salinity transport in the upper ocean appears as a strong northward anomalous transport that rapidly reduces surface salinity south of the circumpolar current (shading in Fig. 8b). As a result, surface density locally decreases, and deep-water production and ocean heat release are suppressed south of 60°S. This effect is larger than in Exp1.0a because the forced salinity anomaly reaches higher amplitudes than what circulation–salinity interaction can accomplish in Fig. 5b. The concurrent decrease of SST (shading in Fig. 8c), primarily due to the reduction of poleward transport of warm upper-ocean water, opposes the surface salinity decrease in controlling the surface density, but again the salinity change is more important. A decrease of SST south of the circumpolar channel also causes significant sea ice expansion and further weakens upward surface heat flux at the poleward edge of the basin (shading in Fig. 8d).

The opening of a circumpolar channel changes the barotropic part of the circulation, but the most significant forced change is in the baroclinic component via slow adjustment of the stratification north of the circumpolar current. The forced transition of deep-water production from the SH to the NH is primarily facilitated by oceanic teleconnection pathways through Kelvin waves along the basin boundaries and at the equator and westward Rossby waves in the basin interior (e.g., Kawase 1987; Johnson and Marshall 2004). The signal from the opening of the circumpolar channel is transmitted northward as a deepening of isopycnals throughout the basin (not shown). The equator acts as a high-frequency filter for deepening of the main pycnocline in the NH (Johnson and Marshall 2004) and thus forces delayed intensification of NH deep-water production there since the large-scale deep-water production rate is proportional to the square of the main pycnocline depth (e.g., Vallis 2006). It takes several decades for anomalous surface salinity and temperature to rise significantly in the NH extratropics in Exp1.3 (Figs. 8b,c).

As in the control experiment Exp1.0a, the anomalous SST rise in the NH extratropics yields the same dominant region of positive surface heat flux anomaly in Exp1.3, but with stronger amplitude. The opening of the SH circumpolar channel rapidly produces the strongest suppression of ocean heat release south of the circumpolar current (light blue shading in Fig. 8d). While in the NH, the greatest ocean heat release, with a multidecadal delay, takes place around 42°N (yellow shading in Fig. 8d) because there the strongest upper-ocean current anomalies act across the strongest mean SST gradient. Again, the anomalies of net surface heat flux have mostly

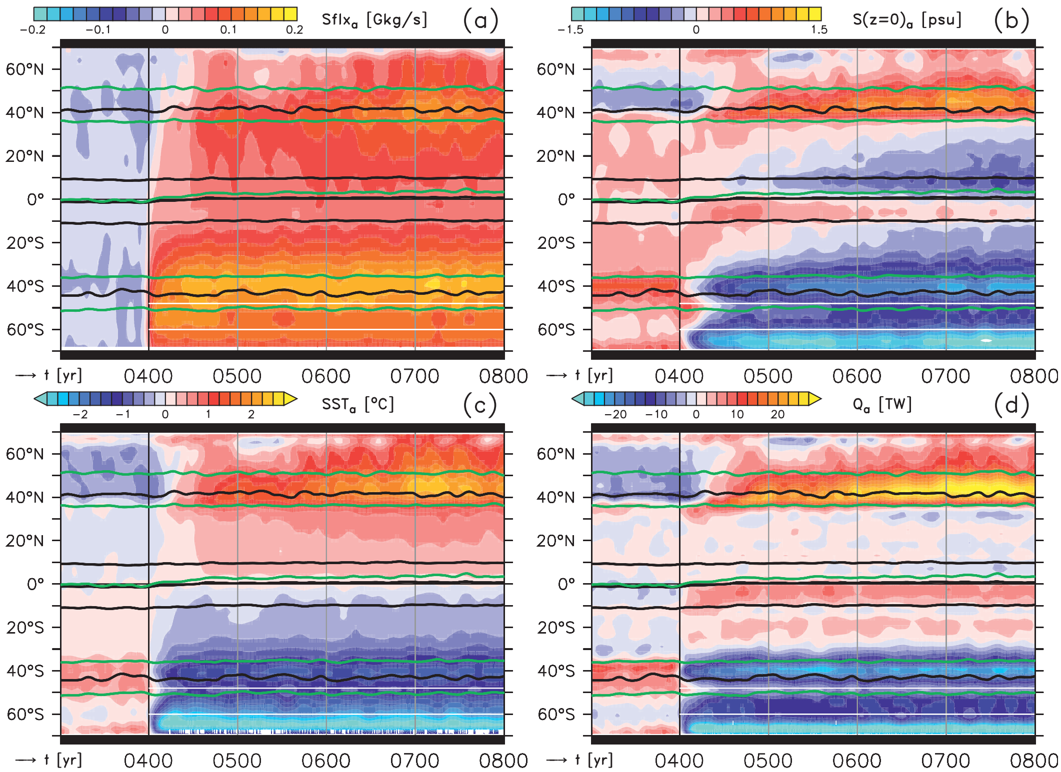

FIG. 8. A key segment of the evolution of anomalous components, with respect to the symmetrized control mean fields, in Exp1.3 bifurcated from Exp1.0 at 01 January 0401 (marked by black horizontal line): (a) anomaly of meridional salinity mass flux zonally and vertically integrated in top 200 m (10^9 kg s^{-1}), (b) zonally averaged anomaly of surface salinity (psu), (c) zonally averaged anomaly of SST (°C), and (d) zonally and 3° meridionally integrated anomaly of net surface heat flux (10^{12} W). The green curves mark zonal mean surface boundaries between the Hadley, Ferrel, and polar cells, while the black curves mark zonal mean boundaries between the tropical, subtropical, and subpolar gyres. The white horizontal lines at 48° and 60°S mark the edges of circumpolar channel. The 31-yr Hamming filter is applied to all fields. The surface heat flux from the ocean to the atmosphere has a positive sign.

opposite signs in the tropics and the extratropics of each hemisphere.

b. Final steady state of a forced experiment

Surface conditions in Exp1.3 evolve to a steady state with asymmetry patterns as shown in Fig. 9. The circumpolar current in the SH disrupts the poleward upper-ocean transport, most importantly along the eastern boundary in the subpolar domain (vectors in Fig. 9a). The surface region of the SH deep-water production is cooled (contours in Fig. 9a) and freshened (shading in Fig. 9a). The resulting decrease of SH deep-water formation is eventually compensated by the intensification of deep-water formation in the NH. The northward orientation of the surface branch of the deep pole-to-pole MOC cell is evident as a strong anomalous northward flow along the western boundary critical for the maintenance of increased (decreased) surface salinity in the NH (SH) extratropics in Fig. 9a. The anomalous northward eastern boundary flow in the NH subpolar domain injects additional salinity into the region of deep-water formation.

The anomalous surface currents again produce the same two key regions of latent heat flux anomalies (contours in Fig. 9b) in the extratropics due to strong anomalous advection across the regions with strong background SST gradient (contours in Fig. 3a). The climate response is similar to the asymmetry in Exp1.0a, but with a stronger magnitude (in the SH due to a circumpolar current and in the NH due to a deeper main pycnocline). In Exp1.3 surface cooling peaks in the southeast corner of the basin (contours in Fig. 9a) because the strongest surface current anomalies are there. The western boundary region around 40°S cools less because there is northward advection of warmer water coming eastward through the circumpolar channel. This water originates at lower latitudes on the western side of the basin. The surface wind asymmetry in Fig. 9b confirms

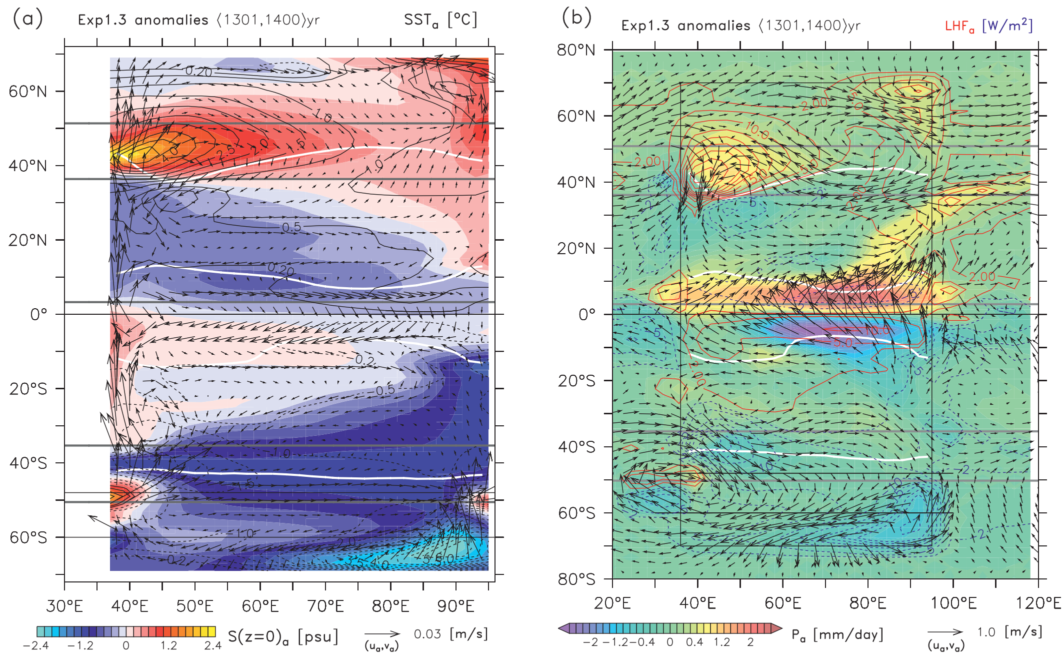

FIG. 9. The steady-state anomalies, with respect to the symmetrized mean control state in Fig. 3, averaged over the last century of Exp1.3. (a) Anomalous SST (contours), anomalous surface salinity (shading), and anomalous surface currents averaged over the top 100 m (vectors). (b) Anomalous latent heat flux [red (positive in the atmosphere) and blue (negative out of the atmosphere) contours], anomalous precipitation (shading), and anomalous surface wind (vectors). The gray horizontal lines mark zonal mean surface boundaries between the Hadley, Ferrel, and polar cells (zonal average of zero meridional surface wind), while the white curves mark boundaries between the tropical, subtropical, and subpolar gyres (zero wind stress curl). The black horizontal lines in the SH subpolar region at 48° and 60°S mark boundaries of the circumpolar channel approximately 2.5 km deep.

that the NH (SH) becomes, in a thermal sense, the summer-like (winter-like) hemisphere with weaker (stronger) winds. The associated asymmetries in SAT, the jet streams, the Hadley circulation, the components of ocean–atmosphere meridional energy transport, and the ITCZ all exhibit similar characteristics as in Exp1.0a, but with a stronger amplitude because of the forced response.

The steady-state MOC streamfunction in Fig. 10 confirms a stronger asymmetry in the deep-MOC cell, with respect to Fig. 2d. The zonally averaged anomalous salinity in Exp1.3 (colored contours in Fig. 10) shows the impact of anomalous northward upper-ocean salinity transport (schematic red arrow in Fig. 10). The SH upper ocean exports salinity to the NH and becomes significantly fresher. In the NH, an intensified deep-water production sequesters the excess in salt below the upper ocean primarily in the southward deep-water flow across the equator.

The surface and interior salinity asymmetry in Exp1.3 is also a direct product of the asymmetry in ocean circulation, because in the extratropics the asymmetry in precipitation (shading in Fig. 9b) opposes the asymmetry in surface salinity (shading in Fig. 9a). The blue and purple arrows in Fig. 10 schematically present the interhemispheric water and heat cycle, respectively, in Exp1.3 (and Exp1.0a). The gray arrows show the cross-equatorial Hadley circulation that is the critical element of interhemispheric thermal interaction caused in our experiments by the asymmetry in deep MOC. The surface branch of the anomalous Hadley cell transports the excess moisture into the warmed hemisphere, where coupled ocean–atmosphere dynamics establish the maximum of tropical precipitation (vertical blue lines in Fig. 10 schematically point to the position of ITCZ).

c. *Climate sensitivity to sill depth of a circumpolar channel*

We now investigate the degree of climate asymmetry subject to changes in the sill depth of the circumpolar channel also motivated by plate tectonics of the earth's lithosphere. Comparison of Exp1.1, Exp1.2, Exp1.3, and Exp1.4 with SH sill depths of 102, 480, 2436, and 3900 m (basin bottom), respectively, enables us to examine the forced change in the upper-ocean meridional salinity transport and its role in the deep MOC and tropical climate asymmetry.

The vertical distributions of zonally integrated anomalous meridional salinity transport in Fig. 11 (shading) show

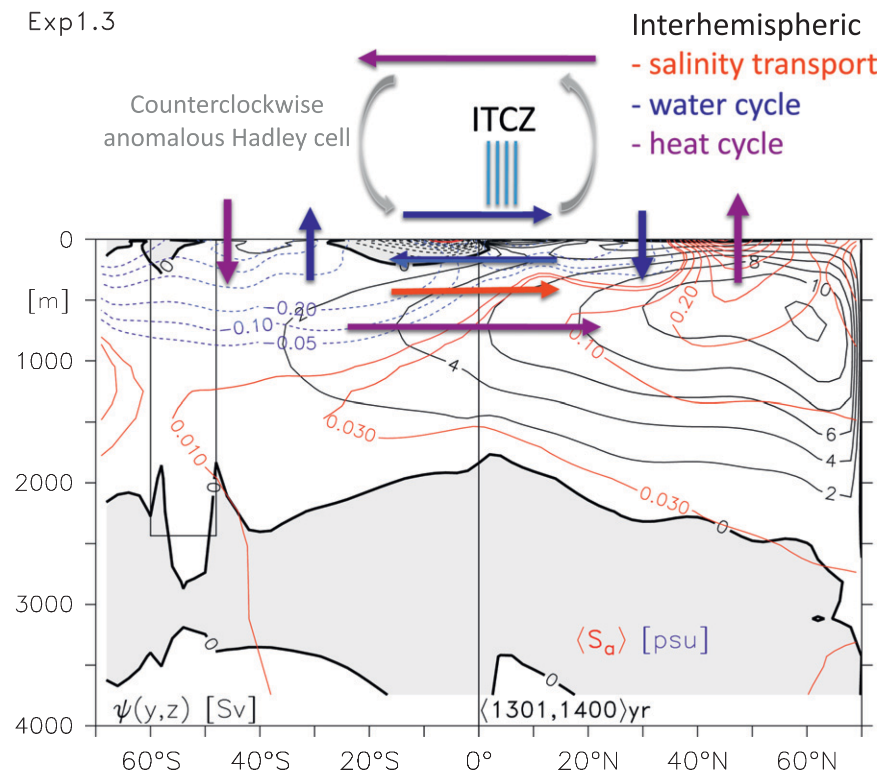

FIG. 10. The final steady state, averaged over the last 100 yr, of Exp1.3 with the SH circumpolar channel 2436 m deep. The black contours and gray shading show the MOC overturning streamfunction overlaid by red (positive) and blue (negative) contours of zonally averaged salinity anomaly (with the respect to the symmetrized mean control state). The red, blue, purple, and gray arrows schematically depict interhemispheric upper-ocean salinity transport, anomalous freshwater transport, anomalous heat transport, and anomalous Hadley circulation, respectively.

the most significant change occurs from Exp1.0 to Exp1.2. Exp1.4 (not shown) produces results very similar to Exp1.3. The upper-ocean subtropical domain is the region with the highest salinity content; hence, the strong poleward advection of salinity in the upper ocean exerts substantial influence over salinity in the subpolar region. When a circumpolar channel completely blocks the main pycnocline (roughly top 500 m) and thus suppresses the geostrophic part of the upper-ocean meridional transport as much as possible, further deepening of the sill level cannot induce a relevant decrease in the salinity poleward of the circumpolar current (contours in Fig. 11). Therefore, the local deep-water production cannot be reduced further as we continue to lower the sill level all the way to the ocean bottom in our model. Below the sill level at 102 m in Exp1.1 there is still a nonnegligible net geostrophic component of the poleward upper-ocean flow. The steady-state MOC streamfunction of Exp1.2, Exp1.3, and Exp1.4 are essentially indistinguishable, while Exp1.1 has a similar but weaker pole-to-pole deep-MOC cell (not shown).

The evolution of the deep-MOC asymmetry in Exp1.2 (green curve), Exp1.3 (blue curve), and Exp1.4 (brown curve) in Fig. 12a is nearly identical after the opening of their circumpolar channels. These three experiments manifest the same multidecadal time scale for the transition of deep-water source from the SH in Exp1.0 to the NH. Exp1.1 (red curve in Fig. 12a) develops a weaker deep-water production in the NH on an even longer time scale. In Exp1.1 below the sill there is still a sufficient amount of the subtropical upper-ocean high-salinity water advected southward, which prevents an almost complete shutdown of the SH deep-water production.

The MOC and ocean state asymmetry dependence on the circumpolar channel sill depth is projected throughout the coupled global climate. The net surface heat flux asymmetry in the extratropics (Fig. 12b) closely follows the deep-MOC asymmetry (Fig. 12a). The tropical ocean–atmosphere domain adjusts to the extratropical surface forcing asymmetry in all experiments by inducing a cross-equatorial Hadley cell as previously discussed.

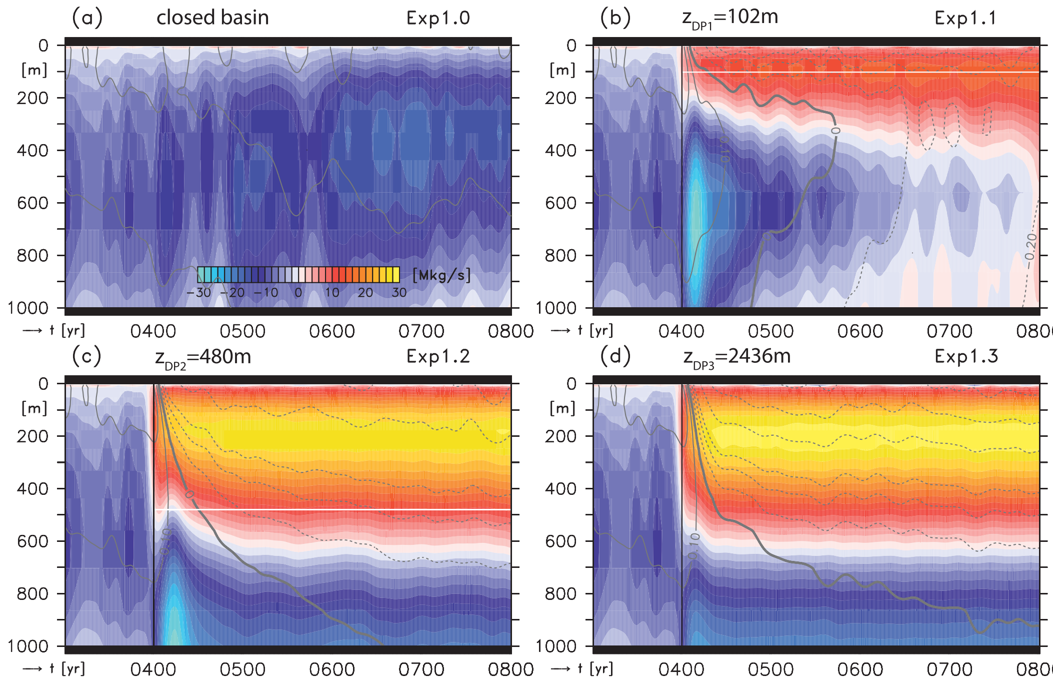

FIG. 11. The shading and contours show development, over the key period, of the vertical distribution of zonally integrated anomalous meridional salinity transport (10^6 kg s^{-1}) at the southern edge of circumpolar channel (60°S) and average salinity anomaly (psu) south of the channel, respectively, in (a) Exp1.0, (b) Exp1.1, (c) Exp1.2, and (d) Exp1.3 in the top 1 km. The black vertical lines mark the opening of circumpolar channels at 01 January 0401. The white horizontal lines in (b) and (c) show the sill depth at 102 and 480 m, respectively.

Figures 12c and 12d show that the response of zonally averaged surface cross-equatorial wind (i.e., surface branch of the anomalous Hadley cell) and the total tropical precipitation asymmetry, respectively, reflect a similar dependence on the sill depth. In our model the atmosphere cannot distinguish whether a circumpolar channel is 500 m deep or if it reaches all the way to the ocean's bottom: its response is the same. Figure 12 indicates the prevailing linear scaling of all pairs of the presented asymmetry indices.

5. Discussion and summary

We have investigated the connection of interhemispheric asymmetry in the ocean circulation and the tropical climate in an idealized single-basin sector CGCM. The unforced and forced symmetry breaking of the upper-ocean meridional salinity transport in the extratropics leads to a substantial asymmetry in the MOC and ocean state. The asymmetry of surface salinity in the extratropics strives to amplify the deep-MOC asymmetry, while SST asymmetry limits its growth by constraining growth of asymmetry in surface density. The associated asymmetry in the OHT breaks the coupled climate symmetry through the development of the key asymmetries in extratropical surface heat flux. They are structured by the upper-ocean circulation anomalies across a strong background SST gradient in the two distinct regions: the first key region is the extended confluence region of subtropical and subpolar western boundary currents beneath the Ferrel cell and the other is the high-latitude region of deep-water production beneath the polar cell.

The asymmetry in extratropical latent heat flux forces an interhemispheric thermal gradient in the atmosphere that causes a wind asymmetry due to a different meridional surface temperature gradient between the equator and midlatitudes in the two hemispheres. In the warmed (cooled) hemisphere with weaker (stronger) jet stream, the Ferrel and Hadley cells reduce (increase) poleward transport of moist static energy, which in an anomalous sense represents interhemispheric AHT that is mediated across the equator via an anomalous Hadley cell. Its energy transport partially compensates the cross-equatorial OHT (about 30% in our model), while its lower branch causes excess moisture convergence and the maximum of precipitation in the tropics of the warmer hemisphere. The magnitudes of surface thermal anomalies in the extratropics (where source SST anomalies drive surface heat flux anomalies) are significantly bigger than in the tropics (where surface flux anomalies, due to wind anomalies induced from the extratropics, drive SST anomalies).

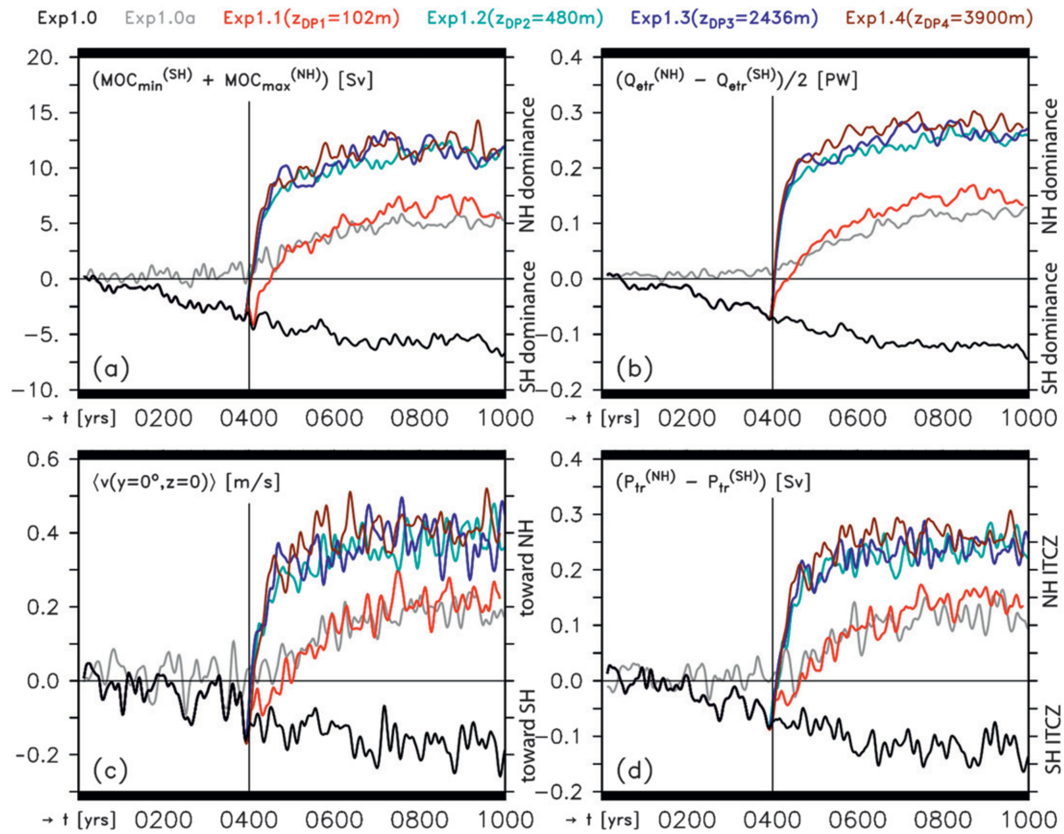

FIG. 12. The time evolution of a set of asymmetry indices, with applied 31-yr Hamming filter, in Exp1.0 (black), Exp1.0a (gray), Exp1.1 (red), Exp1.2 (green), Exp1.3 (blue), and Exp1.4 (brown). (a) The deep-MOC asymmetry (sum of the subpolar MOC streamfunction extrema in both hemispheres). (b) The total asymmetry of extratropical net surface heat flux (with positive sign upward). (c) Zonally averaged surface meridional wind at the equator. (d) The tropical precipitation asymmetry (total tropical precipitation difference between the NH and the SH).

The two symmetric closed-basin simulations (started from different symmetric IC) demonstrate climate bistability because of the advective circulation–salinity feedback that amplifies asymmetry in the upper-ocean meridional salinity transport and the deep MOC. In our model, unforced bistability arises only with hemispheric symmetry in both geometry and annual mean forcing. All explored elements of geometric asymmetry deterministically select the hemisphere containing both the main deep-water source and the ITCZ. Existence of bistability could also depend on the details of numerical setup (e.g., advective scheme or seasonal cycle), since Smith et al. (2006) and Ferreira et al. (2010) did not find bistability in their symmetric configurations.

The set of forced experiments with various circumpolar channels further shows the importance of the upper-ocean meridional salinity transport for the MOC. The opening of a channel in the SH subpolar domain enables the establishment of a circumpolar current that suppresses the poleward transport of salinity and the deep-water formation in the SH. Lowering of the channel sill through the upper part of a water column (roughly top 500 m) substantially alters the MOC and surface heat flux asymmetry, leading to a substantial change in the tropics. Lowering the sill depth below the main pycnocline depth in subtropics produces a saturated response. In the region of a circumpolar current, upwelling driven by the Ekman divergence poleward of the axis of westerlies has a potential to increase ocean heat uptake because it can bring substantial amount of deep cold water to the surface (e.g., Kuhlbrodt et al. 2007). However, in contrast to geometries of Smith et al. (2006) and Ferreira et al. (2010), our circumpolar region is much smaller and narrower, so wind-driven upwelling is not critical for the ocean–atmosphere heat exchange. Also, wind-driven upwelling brings saltier water to the surface that is opposing decrease of surface salinity, but in our setup it cannot overcome the dominant reduction of the upper-ocean poleward salinity transport across the circumpolar current.

6. Conclusions and future directions

Our coupled simulations demonstrate dependence of the main tropical circulation and precipitation (specifically the Hadley circulation and the ITCZ location) on the deep-MOC asymmetry. The main source of deep water and the ITCZ reside in the same hemisphere. The asymmetry indices in Fig. 12 are closely related to the meridional upper-ocean salinity transport in the extratropics. It spontaneously initiates and amplifies the MOC asymmetry in the closed-basin geometry, while it is forced via circumpolar flow in an open-basin geometry. Figure 13a shows that in all experiments (including Exp1.5, which is the equatorially mirrored case from Exp1.3) and in transient and steady states, the interhemispheric difference in the meridional upper-ocean salinity transport, most importantly at the subtropical-subpolar divide (approximately at 42° latitude), is a good linear predictor of the cumulative precipitation asymmetry in the tropics. The anomalous northward (southward) upper-ocean salinity transport yields the NH (SH) deep-water production and the tropical precipitation maximum north (south) of the equator. The horizontal black line in Fig. 13a marks the tropical precipitation asymmetry of Climate Prediction Center (CPC) Merged Analysis of Precipitation (CMAP; Xie and Arkin 1997) 1981–2010 mean, calculated from 80°W to 40°E, indicating that our idealized model with a SH deep circumpolar channel also has some quantitative characteristics of tropical precipitation similar to observations. The water-mass transformation in the extratropics has a significant impact on the tropical pycnocline. Figure 13b shows that in all experiments and all states a more asymmetric deep MOC leads to a deeper and thicker equatorial pycnocline. This behavior reflects the activity of the oceanic wave teleconnection via equatorial Kelvin waves transmitting information about the deep-MOC changes between the hemispheres though changes in depth of isopycnals.

The climate transition from a closed-basin bistability to a circumpolar channel forced asymmetry presents us with the intriguing result that the Southern Ocean circulation and stratification could exert (through the MOC and surface heat flux asymmetry) an important influence over the mean tropical circulation and precipitation. In a general sense, the tropical atmosphere in different regions around the globe is controlled by the superposition of local processes (forced by the top and bottom boundaries) and remote processes (forced by the lateral boundaries). Hence, we are motivated to consider in the follow up study other idealized geometric elements, approximating real-world features, which could have the potential to break the global climate symmetry from the tropics and compete against extratropical forcing agents.

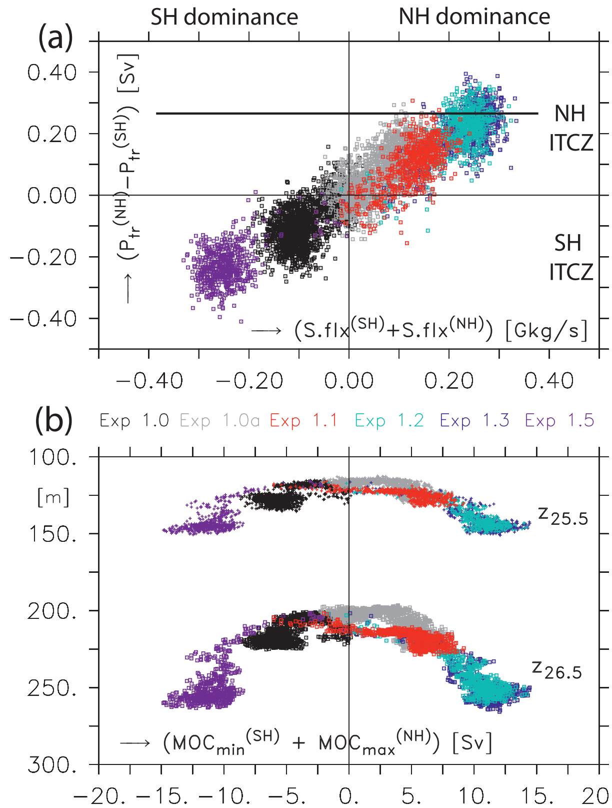

FIG. 13. The climate states, with applied 3-yr Hamming filer, throughout the integration of Exp1.0 (black), Exp1.0a (gray), Exp1.1 (red), Exp1.2 (green), Exp1.3 (blue), and Exp1.5 (purple). (a) The cumulative tropical precipitation difference between the NH and the SH (an ITCZ asymmetry index) as a function of the difference between zonally and vertically integrated meridional salinity transport in the top 200 m at 42°N and at 42°S (average latitude of boundary between the subtropical and subpolar gyres). The vertical line at 0.28 Sv marks the value of ITCZ asymmetry index of CMAP 1981–2010 mean from 80°W to 40°E. (b) Depth of equatorial isopycnals z_x (with x marking sigma densities relative to the surface pressure) averaged between 4°N and 4°S as a function of a deep-MOC asymmetry index (sum of the subpolar MOC streamfunction extrema in both hemispheres) that is proportional to abscissa in (a). Exp1.4 results (not shown) are indistinguishable from Exp1.3 and Exp1.2.

Expansion from single-basin to multibasin configurations would also bring us closer to real-world complexity through the introduction of interbasin interaction and an asymmetric land distribution.

Other potential future directions for investigation are the increase in complexity of atmospheric physics and forcing field in models with various land distributions. With the gray atmosphere we have explored only the minimal dynamic response of the tropical climate to the MOC asymmetry. A diffusive energy balance model can estimate the degree of compensation by the AHT across the equator and top-of-atmosphere (TOA) flux asymmetry

(Kang et al. 2009; Hwang and Frierson 2010; Hwang et al. 2011; Frierson and Hwang 2012). From the atmospheric perspective, a surface heat flux anomaly must be balanced by either TOA flux or by energy transport. The water vapor and cloud feedbacks in a comprehensive AGCM reduce upward longwave radiative transfer and increase asymmetry in surface flux and TOA flux, yielding a higher degree of compensation and a stronger ITCZ shift (Kang et al. 2009). This gives us more confidence in robustness of our result that a circumpolar flow in the extratropics can force the zonal annual mean ITCZ to the opposite hemisphere.

Acknowledgments. This research was supported by the Japan Agency for Marine-Earth Science and Technology (JAMSTEC); by NASA through Grant NNX07AG53G; and by NOAA through Grant NA11NMF4320128, which sponsors research at the International Pacific Research Center. E.A.M. is supported by the Department of Defense (DoD) through the National Defense Science and Engineering Graduate Fellowship (NDSEG) program. D.M.W.F is funded by National Science Foundation (NSF) Grants ATM-0846641 and ATM-0936059.

REFERENCES

Betts, A. K., 1986: A new convective adjustment scheme. Part I: Observational and theoretical basis. *Quart. J. Roy. Meteor. Soc.,* **112,** 677–692.

Broccoli, A. J., K. A. Dahl, and R. J. Stouffer, 2006: Response of the ITCZ to Northern Hemisphere cooling. *Geophys. Res. Lett.,* **33,** L01702, doi:10.1029/2005GL024546.

Broecker, W. S., D. M. Peteet, and D. Rind, 1985: Does the ocean-atmosphere system have more than one stable mode of operation? *Nature,* **315,** 21–26.

Bryan, F., 1986: High-latitude salinity effects and interhemispheric thermohaline circulation. *Nature,* **323,** 301–304.

Chiang, J. C. H., and C. M. Bitz, 2005: Influence of high-latitude ice cover on the marine intertropical convergence zone. *Climate Dyn.,* **25,** 477–496.

——, W. Cheng, and C. M. Bitz, 2008: Fast teleconnections to the tropical Atlantic sector from Atlantic thermohaline adjustment. *Geophys. Res. Lett.,* **35,** L07704, doi:10.1029/2008GL033292.

Cox, M. D., 1989: An idealized model of the World Ocean. Part I: The global-scale water masses. *J. Phys. Oceanogr.,* **19,** 1730–1752.

Dansgaard, W., and Coauthors, 1993: Evidence for general instability of past climate from a 250-kyr ice-core record. *Nature,* **364,** 218–220.

Delworth, T. L., and Coauthors, 2006: GFDL's CM2 global coupled climate models. Part I: Formulation and simulation characteristics. *J. Climate,* **19,** 643–674.

Den Toom, M., H. A. Dijkstra, A. A. Cimatoribus, and S. S. Drijfhout, 2012: Effect of atmospheric feedbacks on the stability of the Atlantic meridional overturning circulation. *J. Climate,* **25,** 4081–4096.

Dijkstra, H. A., and M. J. Molemaker, 1997: Symmetry breaking and overturning oscillations in thermohaline-driven flows. *J. Fluid Mech.,* **331,** 169–198.

——, and M. Ghil, 2005: Low-frequency variability of the large-scale ocean circulation: A dynamical systems approach. *Rev. Geophys.,* **43,** RG3002, doi:10.1029/2002RG000122.

Dima, I. M., and J. M. Wallace, 2003: On the seasonality of the Hadley cell. *J. Atmos. Sci.,* **60,** 1522–1527.

Drijfhout, S. S., 2010: The atmospheric response of a THC collapse: Scaling relations for the Hadley circulation and the nonlinear response in a coupled climate model. *J. Climate,* **23,** 757–774.

Farneti, R., and G. K. Vallis, 2009: An Intermediate Complexity Climate Model (ICCMp1) based on the GFDL flexible modeling system. *Geosci. Model Dev.,* **2,** 73–88.

Ferreira, D., J. Marshall, and J.-M. Campin, 2010: Localization of deep water formation: Role of atmospheric moisture transport and geometrical constraints on ocean circulation. *J. Climate,* **23,** 1456–1476.

Frierson, D. M. W., 2007: The dynamics of idealized convection schemes and their effect on the zonally averaged tropical circulation. *J. Atmos. Sci.,* **64,** 1959–1976.

——, and Y.-T. Hwang, 2012: Extratropical influence on ITCZ shifts in slab ocean simulations of global warming. *J. Climate,* **25,** 720–733.

——, I. M. Held, and P. Zurita-Gotor, 2006: A gray-radiation aquaplanet moist GCM. Part I: Static stability and eddy scales. *J. Atmos. Sci.,* **63,** 2548–2566.

Gent, P., and J. McWilliams, 1990: Isopycnal mixing in ocean circulation models. *J. Phys. Oceanogr.,* **20,** 150–155.

Griffies, S. M., 1998: The Gent–McWilliams skew flux. *J. Phys. Oceanogr.,* **28,** 831–841.

——, M. J. Harrison, R. C. Pacanowski, and A. Rosati, 2004: A technical guide to MOM4. GFDL Ocean Group Tech. Rep. 5, 342 pp.

Grootes, P. M., and M. Stuiver, 1997: Oxygen 18/16 variability in Greenland snow and ice with 10^{-3}- to 10^{-5}-year time resolution. *J. Geophys. Res.,* **102,** 26 455–26 470.

Held, I. M., 2001: The partitioning of the poleward energy transport between the tropical ocean and atmosphere. *J. Atmos. Sci.,* **58,** 943–948.

——, 2005: The gap between simulation and understanding in climate modeling. *Bull. Amer. Meteor. Soc.,* **86,** 1609–1614.

——, and A. Y. Hou, 1980: Nonlinear axially symmetric circulations in a nearly inviscid atmosphere. *J. Atmos. Sci.,* **37,** 515–533.

Hwang, Y.-T., and D. M. W. Frierson, 2010: Increasing atmospheric poleward energy transport with global warming. *Geophys. Res. Lett.,* **37,** L24807, doi:10.1029/2010GL045440.

——, ——, and J. E. Kay, 2011: Coupling between Arctic feedbacks and changes in poleward energy transport. *Geophys. Res. Lett.,* **38,** L17704, doi:10.1029/2011GL048546.

Johnson, H. L., and D. P. Marshall, 2004: Global teleconnections of meridional overturning circulation anomalies. *J. Phys. Oceanogr.,* **34,** 1702–1722.

Kang, S. M., I. M. Held, D. M. W. Frierson, and M. Zhao, 2008: The response of the ITCZ to extratropical thermal forcing: Idealized slab-ocean experiments with a GCM. *J. Climate,* **21,** 3521–3532.

——, D. M. W. Frierson, and I. M. Held, 2009: The tropical response to extratropical thermal forcing in an idealized GCM: The importance of radiative feedbacks and convective parameterization. *J. Atmos. Sci.,* **66,** 2812–2827.

Kawase, M., 1987: Establishment of deep ocean circulation driven by deep-water production. *J. Phys. Oceanogr.,* **17,** 2294–2317.

Koutavas, A., and J. Lynch-Stieglitz, 2004: Variability of the marine ITCZ over the eastern Pacific during the past 30,000 years: Regional perspective and global context. *The Hadley*

Circulation: Present, Past and Future, H. F. Diaz and R. S. Bradley, Eds., Springer, 347–369.

Kuhlbrodt, T., A. Griesel, M. Montoya, A. Levermann, M. Hofmann, and S. Rahmstorf, 2007: On the driving processes of the Atlantic meridional overturning circulation. *Rev. Geophys.,* **45,** RG2001, doi:10.1029/2004RG000166.

Manabe, S., and R. J. Stouffer, 1995: Simulation of abrupt climate change induced by freshwater input to the North Atlantic Ocean. *Nature,* **378,** 165–167.

Marotzke, J., and J. Willebrand, 1991: Multiple equilibria of the global thermohaline circulation. *J. Phys. Oceanogr.,* **21,** 1372–1385.

Peterson, L. C., G. H. Haug, K. A. Hughen, and U. Röhl, 2000: Rapid changes in the hydrologic cycle of the tropical Atlantic during the last glacial. *Science,* **290,** 1947–1951.

Philander, S. G. H., D. Gu, G. Lambert, T. Li, D. Halpern, N.-C. Lau, and R. C. Pacanowski, 1996: Why the ITCZ is mostly north of the equator. *J. Climate,* **9,** 2958–2972.

Rooth, C., 1982: Hydrology and ocean circulation. *Prog. Oceanogr.,* **11,** 131–149.

Sijp, W. P., and M. H. England, 2004: Effect of the Drake Passage throughflow on global climate. *J. Phys. Oceanogr.,* **34,** 1254–1266.

Smith, R. S., C. Dubois, and J. Marotzke, 2006: Global climate and ocean circulation on an aquaplanet ocean–atmosphere general circulation model. *J. Climate,* **19,** 4719–4737.

Stommel, H., 1961: Thermohaline convection with two stable regimes of flow. *Tellus,* **2,** 224–230.

Timmermann, A., and Coauthors, 2007: The influence of a weakening of the Atlantic meridional overturning circulation on ENSO. *J. Climate,* **20,** 4899–4919.

Toggweiler, J. R., and H. Bjornsson, 2000: Drake Passage and paleoclimate. *J. Quat. Sci.,* **15,** 319–328.

Trenberth, K. E., and D. P. Stepaniak, 2003: Seamless poleward atmospheric energy transports and implications for the Hadley circulation. *J. Climate,* **16,** 3706–3722.

Vallis, G. K., 2006: *Atmospheric and Oceanic Fluid Dynamics: Fundamentals and Large-Scale Circulation.* Cambridge University Press, 745 pp.

——, and R. Farneti, 2009: Meridional energy transport in the coupled atmosphere–ocean system: Scaling and numerical experiments. *Quart. J. Roy. Meteor. Soc.,* **135,** 1643–1660.

Wang, X., A. S. Auler, R. L. Edwards, H. Cheng, P. S. Cristalli, P. L. Smart, D. A. Richards, and C.-C. Shen, 2004: Wet periods in northeastern Brazil over the past 210 kyr linked to distant climate anomalies. *Nature,* **432,** 740–743.

Webster, P. J., 2004: The elementary Hadley circulation. *The Hadley Circulation: Present, Past and Future,* H. F. Diaz and R. S. Bradley, Eds., Springer, 9–60.

Winton, M., 2000: A reformulated three-layer sea ice model. *J. Atmos. Oceanic Technol.,* **17,** 525–531.

Xie, P., and P. A. Arkin, 1997: Global precipitation: A 17-year monthly analysis based on gauge observations, satellite estimates, and numerical model outputs. *Bull. Amer. Meteor. Soc.,* **78,** 2539–2558.

Xie, S.-P., 2004: The shape of continents, air-sea interaction and the rising branch of the Hadley circulation. *The Hadley Circulation: Present, Past and Future,* H. F. Diaz and R. S. Bradley, Eds., Springer, 121–152.

——, and S. G. H. Philander, 1994: A coupled ocean-atmosphere model of relevance to the ITCZ in the eastern Pacific. *Tellus,* **46A,** 340–350.

Yoshimori, M., and A. J. Broccoli, 2008: Equilibrium response of an atmosphere–mixed layer ocean model to different radiative forcing agents: Global and zonal mean response. *J. Climate,* **21,** 4399–4423.

Zhang, R., and T. L. Delworth, 2005: Simulated tropical response to a substantial weakening of the Atlantic thermohaline circulation. *J. Climate,* **18,** 1853–1860.